BNL-211767-2019-JAAM

Three-dimensional characterization of hardened paste of hydrated tricalcium silicate by serial block-face scanning electron microscopy

Y. Zhao, I. Robinson

To be published in "Materials"

June 2019

Condensed Matter Physics and Materials Science Department

Brookhaven National Laboratory

U.S. Department of Energy

USDOE Office of Science (SC), Basic Energy Sciences (BES) (SC-22)

DISCLAIMER

Three-dimensional characterization of hardened paste of hydrated tricalcium silicate by serial block-face scanning electron microscopy

Yongjuan Zhao[1], Xianping Liu[1,2,*], Bo Chen[1,3], Fei Yang[1], Yongming Zhang[1], Peiming Wang[1] and Ian Robinson[1,3,4]

[1] School of Materials Science and Engineering, Tongji University, Shanghai 201804, China; 1730602@tongji.edu.cn (Y.Zhao.); bo.chen@tongji.edu.cn (B.Chen.);1610413@tongji.edu.cn (F.Y.); zym126@tongji.edu.cn (Y.Zhang.); tjwpm@126.com (P.W.); i.robinson@ucl.ac.uk (I.R.)

[2] Key Laboratory of Advanced Civil Engineering Materials (Tongji University), Ministry of Education, Shanghai 201804, China

[3] London Centre for Nanotechnology, University College London, London WC1H 0AH, UK

[4] Division of Condensed Matter Physics and Materials Science, Brookhaven National Laboratory, Upton, NY 11973, USA

* Correspondence: lxp@tongji.edu.cn; Tel.: +86-021-3952-6230

Abstract: With the application of a 3D characterization technique, SBFSEM, the 3D microstructure of a hydrated cement monomineral, tricalcium silicate (C3S), was measured with nanoscale resolution. The 3D morphology of unhydrated particles, hydrated products and capillary pores were visualized. Closed and open pores were discovered inside an anhydrous particle. The size and distribution of both the anhydrous C3S particles and its capillary pores were analyzed quantitatively to determine the pore porosity to be 9%. The distribution of pores is found to be in good agreement with the inner and outer product model of Hu et. al, with an inner shell distance of 860 nm. . Considering the spatial resolution of the instrument and large volume of sample probed, most pores can be characterized in this experiment as capillary pores.

Key words: Tricalcium silicate (C3S); Hydration; 3D microstructure; SBFSEM

1. Introduction

Tricalcium silicate (C3S)[1] as the main component in Portland cement taking up 50-70% of cement mass. The hydration reaction occurs between C3S powders and water to form two products, calcium hydroxide (CH) and calcium silicate hydrate (C-S-H)[2, 3]. C3S is attributed with the early-age strength of hardened cement paste of which the hydration degree can reach 70% within 28 days[4, 5]. For this reason, the hydration of C3S has been investigated for several decades[6] and the hydration mechanism has been revealed to a great extent. During that period, a variety of techniques have been developed to reveal the influence of material component and microstructure on macroscopic performance and hence further enrich the hydration mechanism. Some visualization methods such as SEM[7-11], TEM[12-14], AFM[15, 16] have played an important role in the process, including various newly developed three-dimensional visualization techniques such as X-ray computed tomography (CT) [2, 17-21].

Three-dimensional (3D) visualization techniques have great significance in the study of the microstructure of hardened pastes, compared with other more traditional techniques. For

example, while XRD[7, 22-24] and thermal analysis[25, 26] can be used to analyze the average chemical components and hydration degree of a whole sample, CT can be used to analyze the 3D morphology and distribution of independent micro regions[2, 27], which is essential for heterogeneous materials like cement. Compared with 2D techniques such as SEM and TEM, 3D techniques have an advantage of revealing the spatial distribution and the real morphology of irregular-shape phase. In addition, 3D techniques are better than mercury intrusion porosimetry (MIP) in the investigation of pore morphology and pore connectivity[28, 29] although MIP is still the traditional way to measure the pore structure with the size from 1nm to 1000μm[30].

Just like X-ray tomography, serial block-face scanning electron microscopy (SBFSEM) is also a native kind of 3D visualization technique[31]. The concept of SBFSEM was put forward in 1981[31] and the system of SBFSEM was developed by Denk in 2004[32]. While SBFSEM was developed for use in life science, Zankel[33] applied SBFSEM to the study of 3D microstructures of materials in 2009. SBFSEM has widespread potential applications in material science. It has been reported that SBFSEM has been used to image and analyse the 3D microstructures of internal voids, chemical compositions, crack morphology distribution and interfacial bonding of macromolecular materials[34, 35], aluminum alloys[36, 37], zeolite[38] among others. As a 3D technique, SBFSEM has the same advantage laboratory X-ray computed tomography (LCT) has over traditional analysis techniques, but SBFSEM has the additional advantage of higher resolution over LCT, believed to reach about 10-15nm/pixel[34].

This current work extends our previous study of C3S powders with SBFSEM[39] to the hardened paste of hydrated C3S. This expands the application fields of SBFSEM in inorganic, brittle and heterogeneous materials and demonstrates 3D information on the nanometer scale for the microstructure of hardened cement paste. We observed the 3D morphologies of anhydrous C3S, hydrates and pore structure of C3S after 24 hours hydration. The pore size distributions, hydration degree of C3S, porosity and diameter of the pores have been documented qualitatively.

2. Materials and Methods

Monoclinic C3S was manufactured by high sintering according to the methods of De la Torre et al [40] and ground into powder before hydration. The purity of the raw material measured by the Rietvelt method was above 98%. The synthetic C3S was hydrated with a ratio of water to C3S powder (w/c) of 0.5 at 20°C for 24 hours. Because of the restricted sample volume allowed for SBFSEM, the hydration of C3S was conducted in two steps. Firstly, C3S was hydrated in a sealed plastic tube for 5 hours. Then it was removed from the tube and broken into several smaller particles. Finally the particles were allowed to continue to hydrate at 20°C and 60% relative humidity for 19 hours longer.

The hydration was then stopped by infusion with anhydrous ethanol. It was embedded with Agar100 epoxy at the curing temperature of 60°C and curing time of 48h. The sample was trimmed into a frustum-pyramid shape (length of top surface < 500μm, height < 1mm) using a Leica ultramicrotome and fixed on the sample holder with superglue for 2 hours. Conductive silver adhesive was applied around the surface of the sample in order to increase its conductivity.

Backscattered electron (BSE) images of a series of cross sections of the sample were obtained with a Zeiss Sigma VP scanning electron microscope system equipped with a Gatan "3View" in-chamber ultramicrotome. A Gatan "onpoint" backscattered electron detector was used to measure a series of images from each new section of the sample cut by ultramicrotome. Data were collected in high vacuum mode with a 1.5 kV accelerating voltage and 2us/pixel dwell time,, selected to reduce the charging issues caused by the

non-conductivity of the newly cut sections of the sample. An image stack with a 50nm/pixel and 15nm thickness was obtained.

In order to increase the computation speed, original images of 2048×2048 were converted into 1024×1024 using imageJ. Two image stacks obtained from the above procedure were imported into Avizo version 9.4.0 separately for image processing, reconstruction and analysis. The image stacks were processed with the "non-local filter" module and the "align slice" module before image segmentation. Semi-automatic segmentation and manual segmentation were used in combination to increase the accuracy. "Label analysis", "surface distance" and "volume fraction" modules were used for quantitative analysis.

3. Results and Discussion

3.1. The 3D microstructure of hardened paste of hydrated C3S

The BSE image of the first section of the hardened paste of C3S hydrated for 24h is shown in figure 1a. A 3D-rendered image obtained from 380 slices is shown in figure 1b. According to the atomic number or Z-contrast in the BSE image of figure 1a, in which the bright features are anhydrous C3S particles, the grey features are hydrates and the dark features are pores and spaces filled with epoxy. These three features are rendered in blue, grey and green respectively in figure 1b. Rendered 3D images of anhydrous C3S particles and pores, shown in Figure 1c and 1d, have been qualitatively and quantitatively analyzed to further understand the microstructure characteristics of hardened paste in 3D.

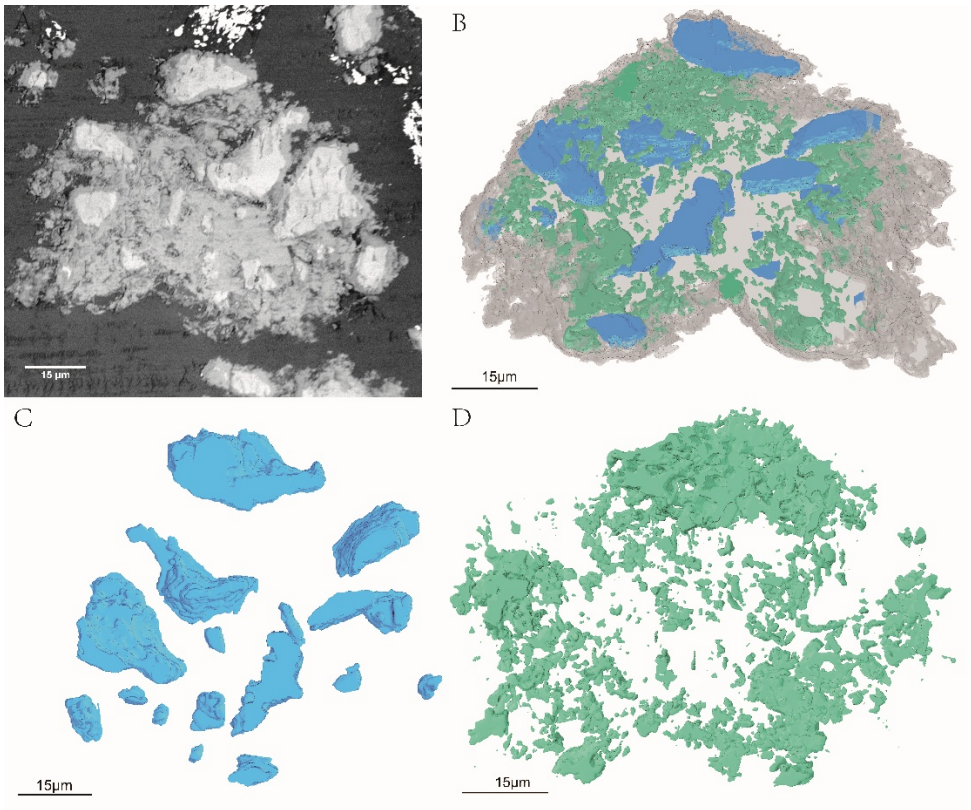

Figure 1. 2D and 3D rendered image of hydrated C_3S: (a) the original backscattered electric (BSE) image of samples; the 3D rendered image of the sample (b), anhydrous particles(c) and pores(d).

3.2. Analysis of anhydrous C3S particles

3.2.1 Morphological parameters of anhydrous C3S

Figure 2a is a labeled 3D image of the segmented anhydrous C3S particles, in which each anhydrous particle is assigned with an ID number from 1 to 18. Basic morphological parameters were analyzed using the 'label analysis' module in Avizo to provide the "volume3d", "area3d", "specific surface area" and "EqDiameter" of all anhydrous particles. The analysis results are shown in supplementary spreadsheet S1 and in figure 2b. The volume ranges from 1.26×10^{6} nm^3 to 1.3×10^{9} nm^3. The EqDiameter of the anhydrous particle ranges 2500 nm to 12500 nm, calculated from the equivalent spherical diameter, hence consistent with the volume change. The area3D changes with the morphology, resulting in the fluctuations in the specific surface area. The general trend is that smaller particles have larger specific surface areas. It is believed that the higher the specific area, the higher the hydration rate.

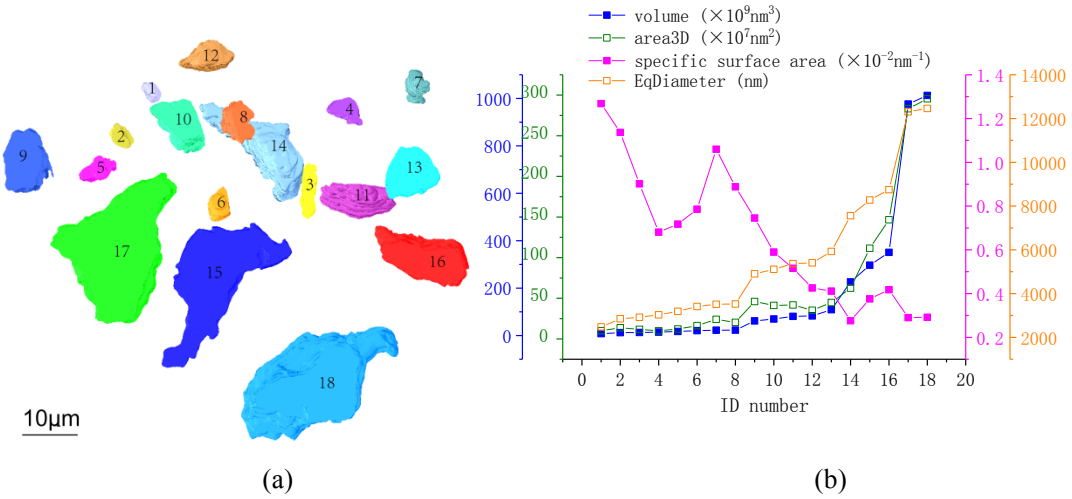

Figure 2. 3D image and quantitative analysis of anhydrous particles: (a) labeled 3D images of anhydrous particles; (b) The volume, area3D, specific surface area and EqDiameter analysis of anhydrous C_3S particles.

3.2.2 Interface structure between Anhydrous C3S particle and hydrates

Figure 3a displays the binary image and a 3D image of another region of the sample with higher resolution. The lateral (x and y) resolution of these data is 20 nm while the depth (z) resolution is 15 nm. The interface between anhydrous C3S particle in light blue and hydrates in dark blue is relatively vulnerable compared with the matrix but of great importance . Although SBFSEM technology is a destructive method, the interface between unhydrated particles and hydrates can be characterised perfectly without any damage as showed in figure 4a when the cutting thickness was 15nm. The inner hydrate layer surrounding anhydrous C3S particles and outer hydrates in the space between unhydrated C3S particles can be clearly seen.

As we can see in figure 4a, two anhydrous particles are separated from each other along with the surrounding hydration products in slice 1. The hydrated products of the two anhydrous particles start to become connected in slice 92 and totally connected in slice 180. The two anhydrous particles themselves begin to join togther in slice 279 and come to a whole particle in slice 281. The 3D image of this region shows that the two anhydrous C3S particles presented in figure 4a slice 1 are in fact part of a single curved particle in figure 4b. It would be easy to come to a wrong conclusion if we had analyzed the structure with just one 2D BSE image like slice 1. Figure 4 illustrates the advantage of SBFSEM over 2D BSE image technology in the accuracy of characterization of the degree of phase morphology. In conclusion, SBFSEM can reveal the uniquely 3D characteristics of the morphology, which

playes an important role in revealing the relationship between microstructure and performance of materials.

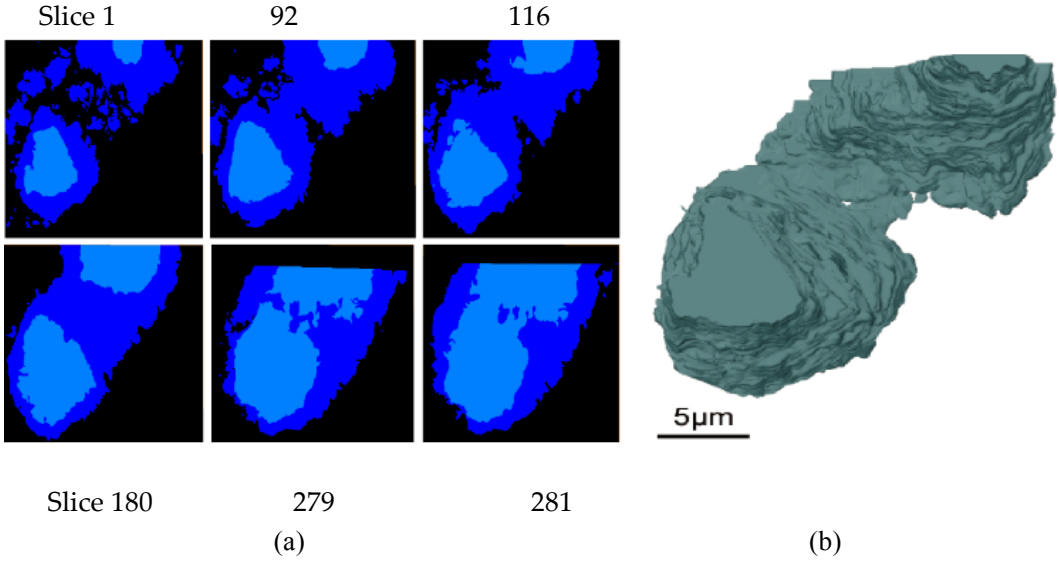

Figure 3. Binary image and 3D image of hydrated C_3S: (a)Binary images of numbered slices; (b) 3D image of an anhydrous particle.

3.3 Analysis of pore structure

3.3.1 Quantitative Analysis of Pores

Pores are one of the most important microstructure characteristics of cement paste, and the Avizo tools are powerful for studying them in 3D. Figure 5a demonstrates the 3D pore network in the hydrates of Figure 1. There are 5200 pores altogether. The large pore cluster rendered in green color is a connected pore, which was separated from the other pores though 'axis connective' module (parameter setting: z-axis; pixel>26). The porosity of connected pores is related to the water transportation ability of the material, which will affect further hydration of anhydrous C3S particles. The porosity of the sample is about 9% of which connected porosity takes up 4.45%. The pore volume, specific surface area and pore EqDiameter were analyzed quantitatively with results listed in supplementary spreadsheet S2. The volume of pores ranged from 1.2×10^{6} nm^3 to 2.0×10^{11} nm^3. The range of pore EqDiameter was between 200 nm and 15000 nm, and 99.7% of pore EqDiameters were below 2000 nm.

The lognormal distribution of pore volume and frequency distribution of pore EqDiameter (<2000nm) are listed in supplementary spreadsheet S2 and shown in figure 5b and 5c. The average pore volume was 1.7×10^{7} nm^3. The 95% confidence interval of the volume logarithmic distribution was (7.224, 7.260) which means 95% particles are between 1.6×10^{7} nm^3 and 1.8×10^{7} nm^3. The average EqDiameter of pores was 380 nm. According to Ma et al's study[10], pores in concrete can be classified into gel pores ranging from 0.5-10nm, capillary pores ranging from 10nm to 10um and macro pores above 10um. From figure 5b, nearly all pores in the sample are capillary pores. No macro pores were detected. The size of the gel pore is lower than the spatial resolution of SBFSEM therefore cannot be measured.

The assesment of pores in cement has been studied for several decades, mercury intrusion porosimetry (MIP) is a the widely accepted method to measure open pores ranging from 1nm-1000μm. Although the pore size range that SBFSEM can detect is smaller than that of MIP, it still has great advantage in the study of the capillary pore structure of cement-based materials. Compared with MIP, SBFSEM can obtain not only the size distribution but also morphology and connectivity parameters of both open pores and closed

pores. Since capillary pores play an important role in the strength, permeability and shrinkage properties of hardened cement paste, their accurate characterization is of great practical significance. From the MIP results of former literatures, the porosities of typical cement materials are between 10% and 40% [41], but the porosity of our sample is about 9%. Although the porosity seen by SBFSEM is in the range of 10%-40%, this apparent agreement is coincidental in consideration of the different pore types the two methods can detect. While MIP can detect gel pores, callirary pores and macro pores, SBFSEM can detect both closed and open pores. The poor imaging quality of SBFSEM, caused by the weak conductivity of samples and the cutting thickness along the z-axis, the spatial resolution for pores is around 50 nm in this study. Measures can be taken to futher improve the spatial resolution of SBFSEM, such as improving the conductivity of epoxy[38], to get closer to the theoretical value of several nanometers.

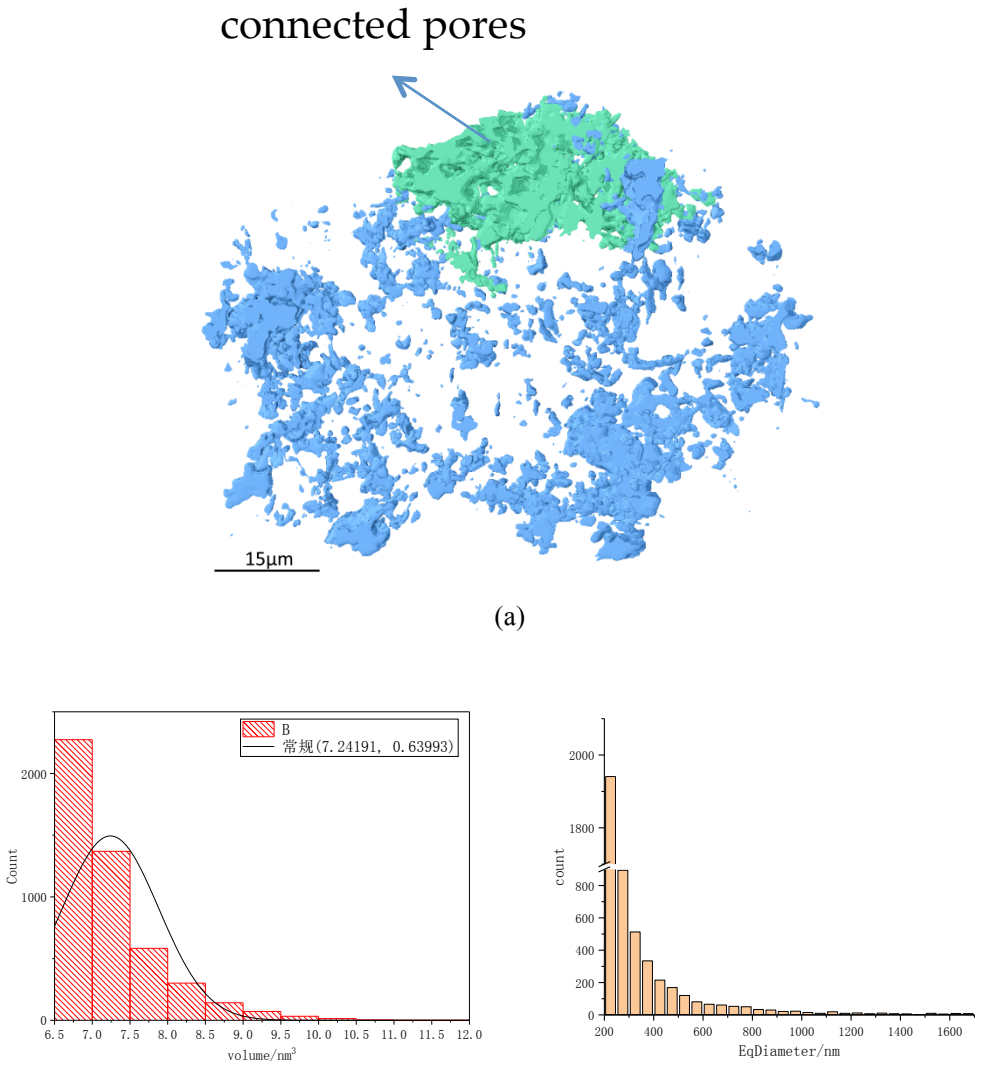

Figure 4. 3D rendered image and analysis of pores: (a) 3D image of connected pores rendered in green and non-connective pores rendered in blue; (b) the volume distribution of all pores; (c) the EqDimeter distribution of all pores.

3.3.2. The spatial distribution of pores

Additional pores were found to be located in the anhydrous particle of No.17, labelled in figure 2a. These are believed to occur by sublimation during the solid phase sintering and are displayed in figure 5. Figure 5a presents the closed pore while in figure 6b, the anhydrous particles, hydrates and pores in the anhydrous particle are displayed separately in transparent gray, blue, and purple colors. The pore located next to the boundary of the anhydrous particle is mostly surrounded by hydrates. And hydrates can also be viewed within a certain thickness of the inner wall of the pore. This arrangement suggests that the pore is more like an open pore than closed.

Open pores have an important relationship with water transportation and hence hydration. Given that hydrates lie at the inner wall of the pore rather than filling the whole pore, the suggests this may have originated as closed pore (filled with air) in the anhydrous C3S particle. During hydration, this closed pore opened and the hydration reaction started at the interface between pores and hydrates and then gradually deposited around the inside of the pore.

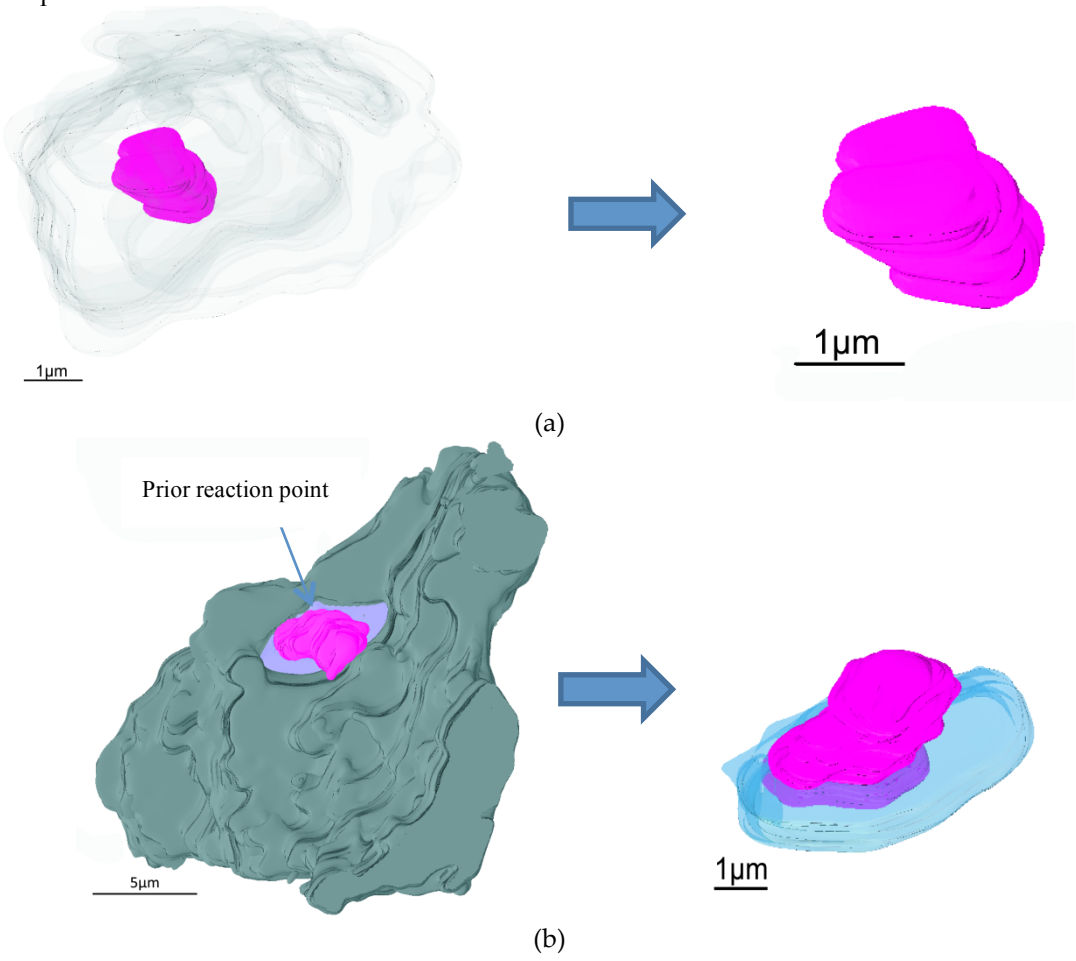

Figure 5. Two types pores in the anhydrous C_3S particles: (a) closed pores; (b) open pores.

The distance from the capillary pores to the surface of the anhydrous particle was computed through 'surface distance' Avizo module which estimates the distance from each voxel on surface 1 to each voxel on surface 2. To assist the distance computation, a small anhydrous particle, No. 2 in fig 2a, was chosen and image was cropped into a 15μm×14μm region. Results are displayed in figure 6 and table 1, as well as in supplementary spreadsheet S3. In figure 6 the pore network around the anhydrous particles is visualized using the shade of color to represent the distance from the anhydrous particle. The shortest distance between the pores and the anhydrous particlesis 30 nm, and the mean value is 4400 nm (table 1). Distances below 860 nm make up only 0.4% of all pixels which means that almost all

capillary pores are located more than 860 nm away from the anhydrous particle. According to Hu et al's study[2], the hydration products can be divided into inner hydration products (IP) with high density and outer hydration products (OP) with low density. Figure 1a shows clearly the difference of pore structure between IP and OP in the BSE image. Capillary pores tend to be found in the OP rather than IP. , The demarcation between the IP and OP of the anhydrous particle can be better identified using the spatial distribution of capillary pores [42] even though they are difficult to distinguish through gray levels. From the above analysis, the thickness of IP is 860 nm, and the OP starts 860 nm away. This analysis method can be used to identify the IP and OP using SBFSEM quantitatively. This new information will be of benefit to the research on 3D microstructure evolution during cement hydration and hence improve our knowledge of the hydration mechanism.

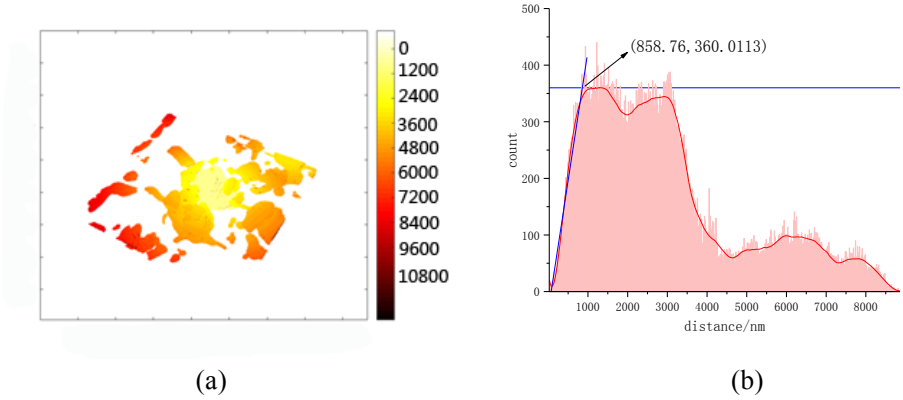

Figure 6. Distance of capillary pores from the surface of the anhydrous C_3S particle qualitatively (a) and quantitatively displayed (b).

Tabel 1 The critical distance from pores to anhydrous particles

	min	mean	max	inflexion
Distance/nm	30	4400	9000	860

4. Conclusions

A novel 3D characterization technique, SBFSEM, was successfully applied to characterize the 3D microstructure of, C3S hydrated for 24 hours, which is a brittle, hard and porous inorganic material,. Due to the poor conductivity of inorganic material, the spatial resolution in this study is limited to 50nm which still makes it possible to observe the 3D microstructure of materials at nanoscale. The morphology, size and distribution of anhydrous particles, hydrates and pores have been analyzed qualitatively and quantitatively. The volume of anhydrous C3S particles ranged from 1.26×10^6 nm^3 to 1.3×10^9 nm^3. The Avizo "EqDiameter" of the anhydrous particles ranged from 2500nm to 12500nm. The above results are essential to the study of hydration kinetics of C3S particles. The volume of pores ranged from $1.6\times10^7nm^3$ to $1.8\times10^7nm^3$ and their EqDiameter ranged from 200 nm to 15000 nm. Average pore volume and diameter were $1.7\times10^7nm^3$ and 380 nm. The locations of open and closed pores associated with hydrates were found 860 nm away from the anhydrous particles. SBFSEM can be further applied to characterize the evolution of 3D microstructure of hardened cement paste at nanoscale along with the hydration time. The 3D analytical results will help us understand the cement hydration mechanism.

Supplementary Materials: The following supplementary materials are available online at www.mdpi.com/xxx/s1, Spreadsheet S1: volume, area, specific surface area, and diameter of 18 anhydrous C3S particles in Figure 2a; Spreadsheet S2: volume, specific surface area, and diameter of

pores below 2000 nm in Figure 4a.

Author Contributions: X.L., B.C. and I.R. conceived the project. Y.Z. (Yongjuan Zhao), X.L. Y.Z. (Yongming Zhang) and P.W. synthesized the C3S monomineral. Y.Z. (Yongjuan Zhao) prepared the hydrated C3S sample and carried out the SBFSEM experiment. Y.Z. (Yongjuan Zhao), F.Y. and B.C. prepared the epoxy embedded C3S sample to be measured with SBFSEM. Y.Z. (Yongjuan Zhao) and X.L. analyzed the data. Y.Z. (Yongjuan Zhao), X.L. and I.R. wrote the manuscript with contributions from all the other authors.

Funding: This research was supported by the Talent Program "Materials Nano-structure" (Grant No. 190073) at Tongji University, the National Natural Science Foundation of China (Grant No. 51102181), the Joint Funds of the National Natural Science Foundation of China (Grant No.U1534207) and the PuJiang Talent Program (Grant No. 18PJ1410400). Work at Brookhaven National Laboratory was supported by the U.S. Department of Energy, Office of Science, Office of Basic Energy Sciences, under Contract No. DE-SC0012704. Work at UCL was supported by grant BB/H022597/1 from the BBSRC.

Acknowledgments: The SBFSEM measurements were carried out at the School of Materials Science and Engineering, Tongji University, China.
Conflicts of Interest: The authors declare no conflict of interest.

References

1. Richardson, I., *Cement Chemistry*. 3rd edition ed.; ICE Publishing: 2018.
2. Hu, Q.; Aboustait, M.; Kim, T.; Ley, M. T.; Bullard, J. W.; Scherer, G.; Hanan, J. C.; Rose, V.; Winarski, R.; Gelb, J., Direct measurements of 3d structure, chemistry and mass density during the induction period of C3s hydration. *Cement and Concrete Research* **2016,** 89, 14-26.
3. Taylor, H. F. W.; Barret, P.; Brown, P. W.; Double, D. D.; Frohnsdorff, G.; Johansen, V.; Ménétrier-Sorrentino, D.; Odler, I.; Parrott, L. J.; Pommersheim, J. M.; Regourd, M.; Young, J. F., The hydration of tricalcium silicate. *Materials and Structures* **1984,** 17, (6), 457-468.
4. Bullard, J. W.; Jennings, H. M.; Livingston, R. A.; Nonat, A.; Scherer, G. W.; Schweitzer, J. S.; Scrivener, K. L.; Thomas, J. J., Mechanisms of cement hydration. *Cement and Concrete Research* **2011,** 41, (12), 1208-1223.
5. Bullard, J. W.; Jennings, H. M.; Livingston, R. A.; Nonat, A.; Scherer, G. W.; Schweitzer, J. S.; Scrivener, K. L.; Thomas, J. J., Mechanisms of cement hydration. *Cement and Concrete Research* **2010,** 41, (12).
6. Scrivener, K. L.; Nonat, A., Hydration of cementitious materials, present and future. *Cement and Concrete Research* **2011,** 41, (7), 651-665.
7. Esteves, L. P., On the hydration of water-entrained cement–silica systems: Combined SEM, XRD and thermal analysis in cement pastes. *Thermochim. Acta* **2011,** 518, (1), 27-35.
8. Feng, X.; Garboczi, E. J.; Bentz, D. P.; Stutzman, P. E.; Mason, T. O., Estimation of the degree of hydration of blended cement pastes by a scanning electron microscope point-counting procedure. *Cement and Concrete Research* **2004,** 34, (10), 1787-1793.

9. Franus, W.; Panek, R.; Wdowin, M. In *SEM Investigation of Microstructures in Hydration Products of Portland Cement*, 2nd International Multidisciplinary Microscopy and Microanalysis Congress, Cham, 2015//, 2015; Polychroniadis, E. K.; Oral, A. Y.; Ozer, M., Eds. Springer International Publishing: Cham, pp 105-112.
10. Igarashi, S.; Kawamura, M.; Watanabe, A., Analysis of cement pastes and mortars by a combination of backscatter-based SEM image analysis and calculations based on the Powers model. *Cement and Concrete Composites* **2004,** 26, (8), 977-985.
11. Ylmén, R.; Jäglid, U.; Steenari, B.-M.; Panas, I., Early hydration and setting of Portland cement monitored by IR, SEM and Vicat techniques. *Cement and Concrete Research* **2009,** 39, (5), 433-439.
12. Groves, G. W., TEM Studies of Cement Hydration. *MRS Proceedings* **2011,** 85, 3.
13. Richardson, I. G.; Skibsted, J.; Black, L.; Kirkpatrick, R. J., Characterisation of cement hydrate phases by TEM, NMR and Raman spectroscopy. *Advances in Cement Research* **2010,** 22, (4), 233-248.
14. Han, S.; Yan, P.; Liu, R., Study on the hydration product of cement in early age using TEM. *Science China Technological Sciences* **2012,** 55, (8), 2284-2290.
15. Papadakis, V. G.; Pedersen, E. J.; Lindgreen, H., An AFM-SEM investigation of the effect of silica fume and fly ash on cement paste microstructure. *Journal of Materials Science* **1999,** 34, (4), 683-690.
16. Peled, A.; Castro, J.; Weiss, W. J., Atomic force and lateral force microscopy (AFM and LFM) examinations of cement and cement hydration products. *Cement and Concrete Composites* **2013,** 36, 48-55.
17. Chotard, T. J.; Boncoeur-Martel, M. P.; Smith, A.; Dupuy, J. P.; Gault, C., Application of X-ray computed tomography to characterise the early hydration of calcium aluminate cement. *Cement and Concrete Composites* **2003,** 25, (1), 145-152.
18. Hu, Q.; Aboustait, M.; Kim, T.; Ley, M. T.; Hanan, J. C.; Bullard, J.; Winarski, R.; Rose, V., Direct three-dimensional observation of the microstructure and chemistry of C3S hydration. *Cement and Concrete Research* **2016,** 88, 157-169.
19. Gastaldi, D.; Canonico, F.; Capelli, L.; Boccaleri, E.; Milanesio, M.; Palin, L.; Croce, G.; Marone, F.; Mader, K.; Stampanoni, M., In situ tomographic investigation on the early hydration behaviors of cementing systems. *Construction and Building Materials* **2012,** 29, 284-290.
20. Helfen, L.; Dehn, F.; Mikulík, P.; Baumbach, T., Three-dimensional imaging of cement microstructure evolution during hydration. *Advances in Cement Research* **2005,** 17, (3), 103-111.
21. Liu, X.; Aranda, M. A. G.; Chen, B.; Wang, P.; Harder, R.; Robinson, I., In Situ Bragg Coherent Diffraction Imaging Study of a Cement Phase Microcrystal during Hydration. *Crystal Growth & Design* **2015,** 15, (7), 3087-3091.
22. Hesse, C.; Goetz-Neunhoeffer, F.; Neubauer, J., A new approach in quantitative in-situ XRD of cement pastes: Correlation of heat flow curves with early hydration reactions. *Cement and Concrete Research* **2011,** 41, (1), 123-128.
23. Mendes, A.; Gates, W. P.; Sanjayan, J. G.; Collins, F., NMR, XRD, IR and synchrotron NEXAFS spectroscopic studies of OPC and OPC/slag cement paste hydrates. *Materials and Structures* **2011,** 44, (10), 1773-1791.

24. Scrivener, K. L.; Füllmann, T.; Gallucci, E.; Walenta, G.; Bermejo, E., Quantitative study of Portland cement hydration by X-ray diffraction/Rietveld analysis and independent methods. *Cement and Concrete Research* **2004,** 34, (9), 1541-1547.
25. Soin, A. V.; Catalan, L. J. J.; Kinrade, S. D., A combined QXRD/TG method to quantify the phase composition of hydrated Portland cements. *Cement and Concrete Research* **2013,** 48, 17-24.
26. Vedalakshmi, R.; Sundara Raj, A.; Srinivasan, S.; Ganesh Babu, K., Quantification of hydrated cement products of blended cements in low and medium strength concrete using TG and DTA technique. *Thermochim. Acta* **2003,** 407, (1), 49-60.
27. Parisatto, M.; Dalconi, M. C.; Valentini, L.; Artioli, G.; Rack, A.; Tucoulou, R.; Cruciani, G.; Ferrari, G., Examining microstructural evolution of Portland cements by in-situ synchrotron micro-tomography. *Journal of Materials Science* **2015,** 50, (4), 1805-1817.
28. Cook, R. A.; Hover, K. C., Mercury porosimetry of cement-based materials and associated correction factors. *Construction and Building Materials* **1993,** 7, (4), 231-240.
29. Zhang, Y.; Wu, B.; Zhou, J.; Ye, G.; Shui, z., *Pore structure of blended cement paste by means of pressurization–depressurization cycling mercury intrusion porosimetry*. 2014.
30. Ibrahim, M.; Arockiaraj, J.; Amritanand, R.; Venkatesh, K.; David, K. S., Recurrent Lumbar Disc Herniation: Results of Revision Surgery and Assessment of Factors that May Affect the Outcome. A Non-Concurrent Prospective Study. *Asian Spine J.* **2015,** 9, (5), 728-736.
31. Leighton, S. B., SEM images of block faces, cut by a miniature microtome within the SEM - a technical note. *Scan Electron Microsc* **1981**, (Pt 2), 73-76.
32. Denk, W.; Horstmann, H., Serial Block-Face Scanning Electron Microscopy to Reconstruct Three-Dimensional Tissue Nanostructure. *PLOS Biology* **2004,** 2, (11), e329.
33. Zankel, A.; Kraus, B.; Poelt, P.; Schaffer, M.; Ingolic, E., Ultramicrotomy in the ESEM, a versatile method for materials and life sciences. *J. Microsc.*. **2009,** 233, (1), 140-148.
34. Carr, J.; Milhet, X.; Gadaud, P.; Boyer, S. A. E.; Thompson, G. E.; Lee, P., Quantitative characterization of porosity and determination of elastic modulus for sintered micro-silver joints. *Journal of Materials Processing Technology* **2015,** 225, 19-23.
35. Chen, B.; Hashimoto, T.; Vergeer, F.; Burgess, A.; Thompson, G.; Robinson, I., Three-dimensional analysis of the spatial distribution of iron oxide particles in a decorative coating by electron microscopic imaging. *Progress in Organic Coatings* **2014,** 77, (6), 1069-1072.
36. Hashimoto, T.; Curioni, M.; Zhou, X.; Mancuso, J.; Skeldon, P.; Thompson, G. E., Investigation of dealloying by ultra-high-resolution nanotomography. *Surface and Interface Analysis* **2012,** 45, (10), 1548-1552.
37. Lu, J.; Chen, B.; Liu, X.; Yang, F.; Robinson, I. K., 3D microstructure reconstruction of casting aluminum alloy based on serial block-face scanning electron microscopy. *Journal of Alloys and Compounds* **2019,** 778, 721-730.
38. Bai, X.; Chen, B.; Yang, F.; Liu, X. P.; Silva-Nunes, D.; Robinson, I., Three-dimensional imaging and analysis of the internal structure of SAPO-34 zeolite crystals. *RSC Adv.* **2018,** 8, (59), 33631-33636.
39. Yang, F.; Liu, X.; Zhao, Y.; Zhang, Y.; Wang, P.; Robinson, I.; Chen, B., Investigation of Three-Dimensional Microstructure of Tricalcium Silicate (C3S) by Electron Microscopy. *Materials* **2018,** 11, (7), 1110.

40. De la Torre, A. G.; Aranda, M. A. G., Accuracy in Rietveld quantitative phase analysis of Portland cements. *Journal of Applied Crystallography* **2003,** 36, (5), 1169-1176.
41. Wang, Y.-S.; Dai, J.-G., X-ray computed tomography for pore-related characterization and simulation of cement mortar matrix. *NDT & E International* **2017,** 86, 28-35.
42. Bullard, J. W.; Hagedorn, J.; Ley, M. T.; Hu, Q.; Griffin, W.; Terrill, J. E., A Critical Comparison of 3D Experiments and Simulations of Tricalcium Silicate Hydration. *J Am Ceram Soc* **2018,** 101, (4), 1453-1470.